Journal of Molecular Structure 1134 (2017) 649–660

Contents lists available at ScienceDirect

Journal of Molecular Structure

journal homepage: http://www.elsevier.com/locate/molstruc

Structural variety of mono- and binuclear transition metal complexes of 3-[(2-hydroxy-benzylidene)-hydrazono]-1-(2-hydroxyphenyl)-butan-1-one: Synthesis, spectral, thermal, molecular modeling, antimicrobial and antitumor studies

Magdy Shebl [a, *], Omima M.I. Adly [a], Hoda F. El-Shafiy [a], Saied M.E. Khalil [a], A. Taha [a], Mohammed A.N. Mahdi [a, b]

[a] Chemistry Department, Faculty of Education, Ain Shams University, Roxy, Cairo, 11341, Egypt
[b] Department of Industrial Chemistry, Faculty of Applied Science, Hajjah University, Yemen

ARTICLE INFO

Article history:
Received 11 October 2016
Received in revised form
29 December 2016
Accepted 2 January 2017
Available online 4 January 2017

Keywords:
Polydentate Schiff base
Mono- and binuclear complexes
Thermal studies
Molecular modeling
Antimicrobial activity
Antitumor activity

ABSTRACT

A new polydentate Schiff base ligand and its metal complexes were synthesized and characterized by elemental analyses, IR, ^{1}H NMR, electronic, ESR and mass spectra, conductivity and magnetic susceptibility measurements as well as thermal analyses. The free ligand was synthesized by condensation of *o*-acetoacetylphenol with salicylaldehyde hydrazone. The analytical and spectroscopic tools showed that the obtained complexes are mono- and binuclear complexes, which can be generally formulated as: $[(L)M_2X_2(H_2O)_m]\cdot nZ$; M = Cr, Fe, Ni or Cu, X = OAc or NO_3, m = 5 or nil and n = 3, 1.5 or 0.5 and Z = EtOH or H_2O, $[(H_2L)_2M(X)_m].nH_2O$; M = Mn, Zn, or Cd, X = EtOH, H_2O or nil, m = 2 or nil and n = 3.5 or 0, $[(HL)_2Co_2]\cdot 0.5H_2O$ and $[(H_2L)_2UO_2(H_2O)]$. The metal complexes displayed octahedral, tetrahedral and square-planar geometrical arrangements, while uranium complex displayed seven-coordinate. Kinetic parameters (E_a, A, ΔH, ΔS and ΔG) of the thermal decomposition stages have been evaluated using Coats–Redfern equations. The molecular structural parameters of the ligand and its metal complexes have been calculated and correlated with the experimental data such as IR. The antimicrobial activity of the ligand and its complexes was screened against some kinds of bacteria and fungi. The antitumor activity of the ligand and its Ni(II) and Cu(II) complexes was investigated against HepG2 cell line.

1. Introduction

Schiff bases are considered to be the most important ligands in coordination chemistry. They are utilized as catalysts, dyes and pigments, intermediates in organic synthesis and as polymer stabilizers [1]. Furthermore, Schiff bases have been used in the synthesis of a number of industrial and biologically active compounds such as formazans, benzoxazines, and so on [2].

Schiff bases and their complexes have attracted a great interest because of their diverse applications including antimicrobial [3,4], anticancer [5,6], antioxidant [7,8], anti-inflammatory [9], antiviral [10] and herbicidal [11] activities. Also, some complexes of Schiff bases have been used as model molecules for biological oxygen carrier systems [12] as well as possessing analytical applications [13].

Currently, a great interest is being focused on polydentate Schiff bases. This is due to their ability to form varieties of complexes with various stoichiometry, chelating, magnetic and spectral properties [14].

There is a significant interest to synthesize and characterize metal complexes with dicompartmental ligands [15]. This is due to their importance in biomimetic researches of binuclear metalloproteins [16], their interesting catalytic properties [17] as well as their capability to stabilize unusual oxidation states and mixed-valance compounds. Among them, phenol based macrocyclic binucleating ligands containing two different compartments have predominantly received immense consideration as they can bind two metal centers in close proximity [18].

The aim of the current work is to synthesize and characterize a new polydentate Schiff base ligand, 3-[(2-hydroxy-benzylidene)-

* Corresponding author.
E-mail address: magdy_shebl@hotmail.com (M. Shebl).

http://dx.doi.org/10.1016/j.molstruc.2017.01.012
0022-2860/

hydrazono]-1-(2-hydroxyphenyl)-butan-1-one, and its metal complexes with chromium(III), manganese(II), iron(III), cobalt(II), nickel(II), copper(II), zinc(II), cadmium(II) and dioxouranium(VI) ions. The structures of the ligand and its metal complexes were characterized by using elemental and thermal analyses, IR, ^{1}H NMR, electronic, ESR and mass spectra in addition to magnetic susceptibility and conductivity measurements. Molecular modeling was carried out for the ligand and its complexes on the basis of semi-empirical *PM*3 level implemented with *Hyperchem* 7.52 program and the results were correlated with the experimental data. The antimicrobial activity of the ligand and its metal complexes was screened against Gram–positive bacteria (*Staphylococcus aureus* and *Bacillus subtilis*), Gram–negative bacteria (*Salmonella typhimurium* and *Escherichia coli*), yeast (*Candida albicans*) and fungus (*Aspergillus fumigatus*). Finally, the antitumor activity of the ligand and its Ni(II) and Cu(II) complexes was investigated against HepG2 cell line.

2. Experimental

2.1. Reagents and materials

o-Acetoacetylphenol [19] and salicylaldehyde hydrazone [20] were prepared following the literature procedures. Metal acetates, metal indicators, EDTA disodium salt, ammonium hydroxide and nitric acid were either BDH or Merck chemicals. Organic solvents were reagent grade chemicals and were used without further purification.

2.2. Synthesis of the ligand

The new Schiff base (Scheme 1) was prepared by adding *o*-acetoacetylphenol (2 g, 11.24 mmol) to salicylaldehyde hydrazone (1.53 g, 11.24 mmol), both dissolved in absolute ethanol (40 ml). The reaction mixture was heated under reflux for 6 h and a yellow precipitate is formed upon cooling the solution to room temperature. The product was filtered off and washed with few amounts of ethanol then diethyl ether, air-dried and recrystallized from ethanol. The yield was 1.8 g (54%). The physical properties and analytical data of the ligand and its metal complexes are scheduled in Table 1.

2.3. Synthesis of the metal complexes

A hot 30 mL ethanolic solution of the metal salt was gradually added to the solution of the ligand (40 mL) in 1:2 (L:M) molar ratio and the solution was heated under reflux for 7 h during which the solid complex precipitated. The precipitate was filtered off, washed with ethanol or methanol then diethyl ether and finally air-dried. The uranyl complex was prepared in methanol. The following is a procedure example for the synthesis of the copper(II) complex in details.

2.3.1. $[(HL)Cu_2(OAc)_2]\cdot 0.5H_2O$, **6**

To 0.5 g (1.69 mmol) of the ligand dissolved in 30 mL ethanol, was added 0.674 g (3.38 mmol) of $Cu(OAc)_2\cdot H_2O$ dissolved in 30 mL ethanol with stirring. The reaction mixture was heated under reflux for 7 h. The deep brown precipitate was filtered off, washed with ethanol then diethyl ether and finally air-dried. Yield: 0.4 g (54%).

2.4. Analytical and physical measurements

Elemental analyses were carried out using Vario El-Elementar at the Ministry of Defense, Chemical War Department. Analyses of the metal content followed the decomposition of metal complexes with conc. nitric acid then metal ions were estimated by EDTA [21–23]. IR spectra were recorded using KBr discs on FT IR Nicolet 6700 spectrometer. Electronic spectra were recorded for DMF solution or Nujol mulls on a Jasco UV–Vis spectrophotometer model V-550. ^{1}H NMR spectra were recorded at room temperature by using a Bruker WP 200 SY spectrometer of DMSO-d_6, solution and tetramethylsilane (TMS) as an internal reference. D_2O was added to every sample to test for the deutration of the samples. ESR spectra of the complexes were recorded at an Elexsys, E500, Bruker spectrometer. Mass spectra were recorded at 70 eV on a Gas chromatographic GCMSqp 1000 ex Shimadzu instrument. Magnetic susceptibility values were obtained using Johnson Matthey, Alfa product, Model No. (MKI magnetic susceptibility balance). Effective magnetic moments were calculated from the expression $\mu_{eff.} = 2.828\ (\chi_M.T)^{1/2}$ B.M., where χ_M is the molar susceptibility corrected using Pascal's constants for the diamagnetism of all atoms in the compounds [24]. Molar conductivities were measured for 10^{-3} M solution of the solid complexes on the Corning conductivity meter NY 14831 model 441. The TG–DTG measurements were carried out on a Shimadzu thermogravimetric analyzer in dry nitrogen atmosphere with a heating rate of 20 °C/min using the TA-50 WS1 program.

2.5. Antimicrobial activity

The standardized disc-agar diffusion method [25] was followed to determine the activity of the synthesized compounds against the sensitive organisms *Staphylococcus aureus* (ATCC 25923) and *Bacillus subtilis* (ATCC 6635) as Gram positive bacteria, *Salmonella typhimurium* (ATCC 14028) and *Escherichia coli* (ATCC 25922) as Gram negative bacteria and *Candida albicans* (ATCC 10231) and *Aspergillus fumigatus* as fungus strain. The antibiotic chloramphenicol was used as reference in the case of Gram-positive bacteria, cephalothin in the case of Gram-negative bacteria and cycloheximide in the case of fungi.

2.6. Antitumor activity

Cell toxicity was monitored on Hep G2 cells by determining the effect of the test samples on cell morphology and cell viability according to literature method [26].

3. Results and discussion

3.1. The ligand

Table 2 records the characteristic IR spectral data of the Schiff base ligand. The IR spectrum of the ligand showed bands at 3432, 1618 and 1567 cm^{-1} that may be assigned to ν(O–H), ν(C=N) and ν(C=O) + ν(C=C) groups, respectively [27,28].

Electronic spectral data of the ligand in DMF (Table 3) showed two bands at 31,746 and 28,571 cm^{-1}. The first band may be due to π-π^* transitions of the azomethine linkage and the aromatic benzene ring. The second band may be assigned to n-π^* transitions of the C=O and C=N groups and/or charge transfer transitions within the molecule.

^{1}H NMR spectral data of the free ligand, dissolved in DMSO-d_6, displayed two signals at 13.3 and 11.1 ppm, which may be assigned to phenolic OH protons, which were highly de-shielded by attached oxygen atom (Scheme 1). However, the two signals observed at 10.2 and 6.1 ppm may be to OH and NH protons in tautomer III (Scheme 1). Those resonated down the field due to highly desheilding effect from oxygen and nitrogen atom. Whereas, the signals observed at 9, 8.6 and 2.3 ppm were assigned to CH=N, CH=C and methyl protons, respectively. The aromatic protons were observed in the range

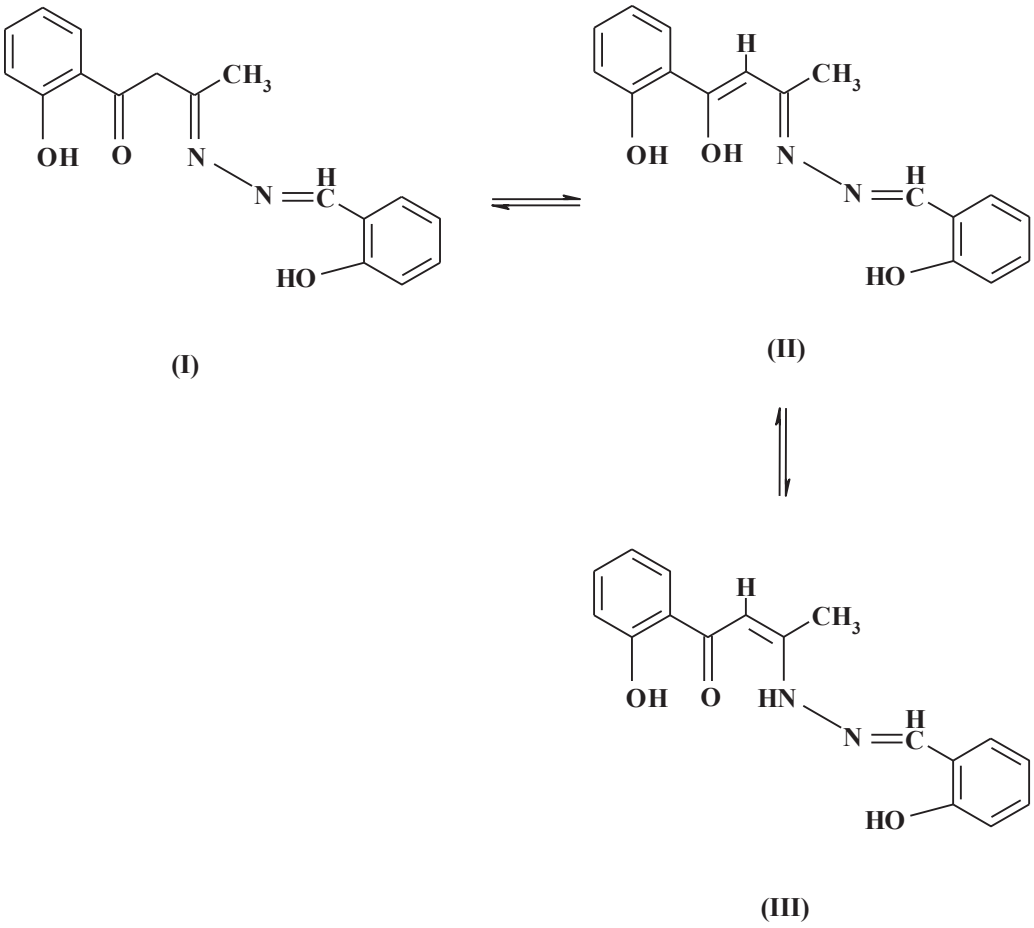

Scheme 1. Tautomeric forms of the Schiff base, H_3L, ligand.

Table 1
Analytical and physical data of the Schiff base ligand and its metal complexes.

No.	Reaction	Complex [M. F.] [F. W.]	Color	Yield (%)	M.P. °C	Elemental analysis, % Found/(calc.)			
						C	H	N	M
	H_3L	$[C_{17}H_{16}N_2O_3]$ [296.33]	Yellow	54	182	68.6 (68.91)	5.2 (5.44)	9.7 (9.45)	–
(1)	$H_3L + Cr(OAc)_2 \cdot H_2O$	$[(L)Cr_2(OAc)_3(H_2O)_5] \cdot 3H_2O$ $[C_{23}H_{38}N_2O_{17}Cr_2]$ [718.55]	Reddish brown	85	>300	38.1 (38.45)	5.0 (5.33)	4.2 (3.9)	14.3 (14.47)
(2)	$H_3L + Mn(OAc)_2 \cdot 4H_2O$	$[(H_2L)_2Mn(EtOH)_2]$ $[C_{38}H_{42}N_4O_8Mn]$ [737.72]	Yellowish brown	45	>300	62.0 (61.87)	5.4 (5.74)	7.9 (7.59)	7.3 (7.45)
(3)	$H_3L + Fe(NO_3)_3 \cdot 9H_2O$	$[(L)Fe_2(NO_3)_3(H_2O)_5] \cdot 1.5H_2O$ $[C_{17}H_{26}N_5O_{18.5}Fe_2]$ [708.11]	Pale brown	58	>300	28.64 (28.84)	3.73 (3.7)	9.6 (9.89)	15.6 (15.77)
(4)	$H_3L + Co(OAc)_2 \cdot 4H_2O$	$[(HL)_2Co_2] \cdot 0.5H_2O$ $[C_{34}H_{29}N_4O_{6.5}Co_2]$ [715.5]	Pale brown	42	>300	56.7 (57.08)	4.15 (4.09)	8.1 (7.83)	16.3 (16.47)
(5)	$H_3L + Ni(OAc)_2 \cdot 4H_2O$	$[(HL)Ni_2(OAc)_2] \cdot 0.5EtOH$ $[C_{22}H_{23}N_2O_{7.5}Ni_2]$ [552.86]	Deep yellow	66	>300	48.1 (47.8)	4.36 (4.19)	5.3 (5.07)	21.0 (21.24)
(6)	$H_3L + Cu(OAc)_2 \cdot H_2O$	$[(HL)Cu_2(OAc)_2] \cdot 0.5H_2O$ $[C_{21}H_{21}N_2O_{7.5}Cu_2]$ [548.5]	Deep brown	54	292	46.3 (45.99)	4.02 (3.86)	5.5 (5.11)	22.8 (23.17)
(7)	$H_3L + Zn(OAc)_2 \cdot 2H_2O$	$[(H_2L)_2Zn]$ $[C_{34}H_{30}N_4O_6Zn]$ [656.01]	Pale yellow	46	214	62.6 (62.25)	4.7 (4.61)	8.9 (8.54)	9.8 (9.96)
(8)	$H_3L + Cd(OAc)_2 \cdot 2H_2O$	$[(H_2L)_2Cd(H_2O)_2] \cdot 3.5H_2O$ $[C_{34}H_{41}N_4O_{11.5}Cd]$ [802.13]	Yellow	44	>300	50.69 (50.91)	4.8 (5.15)	7.3 (6.93)	13.9 (14.01)
(9)	$H_3L + UO_2(OAc)_2 \cdot 2H_2O$	$[(H_2L)_2UO_2(H_2O)]$ $[C_{34}H_{32}N_4O_9U]$ [878.69]	Brick red	80	>300	46.75 (46.48)	4.0 (3.67)	6.06 (6.38)	a (27.09)

a Not determined.

of 6.8–7.9 ppm. Based on ^{1}H NMR spectral data, it was concluded that the ligand exists as tautomers II and III in solution (Scheme 1).

The mass spectrum of the ligand (Fig. 1) showed the molecular ion peak at *m/z* 296 confirming formula weight (F.W 296.33), which was proposed on the basis of micro-analytical data. The mass fragmentation outline, shown in Scheme S1 (Supplementary material), supported the suggested structure of the ligand.

Table 2
Characteristic IR spectral data (cm^{-1}) of the Schiff base, H_3L, ligand and its metal complexes.

No.	Compound / complex	IR Spectra (cm^{-1})						
		νOH (Phenolic + H_2O)	νC = N	$\nu_{C=O} + \nu_{C=C}$	$N_{C=N}$	νM-O	νM-N	Other bands
	H_3L	3432	1618	1567	1483	–	–	–
1	$[(L)Cr_2(OAc)_3(H_2O)_5]\cdot 3H_2O$	3407	1607	1539	1451	580	436	1687; $\nu_{as}(COO^-)$, 1576; $\nu_s(COO^-)$; (monodentate OAc^-)
2	$[(H_2L)_2Mn(EtOH)_2]$	3400	1623	1540	1486	548	422	
3	$[(L)Fe_2(NO_3)_3(H_2O)_5]\cdot 1.5H_2O$	3307	1609	1545	1451	600	494	1384, 1152; $\nu(NO_3^-)$ (monodentate)
4	$[(HL)_2Co_2]\cdot 0.5H_2O$	3392	1610	1540	1470	587	491	
5	$[(HL)Ni_2(OAc)_2]\cdot 0.5EtOH$	3421	1607	1541	1470	502	422	1574; $\nu_{as}(COO^-)$, 1500; $\nu_s(COO^-)$; (bidentate OAc^-)
6	$[(HL)Cu_2(OAc)_2]\cdot 0.5H_2O$	3246	1609	1534	1466	501	419	1586; $\nu_{as}(COO^-)$, 1507; $\nu_s(COO^-)$; (bidentate OAc^-)
7	$[(H_2L)_2Zn]$	3240	1620	1530	1484	548	421	
8	$[(H_2L)_2Cd(H_2O)_2]\cdot 3.5H_2O$	3408	1623	1544	1470	502	471	
9	$[(H_2L)_2UO_2(H_2O)]$	3432	1621	1551	1492	501	436	917; ν(O=U=O)

Table 3
Electronic spectra, magnetic moments and molar conductivity data of the Schiff base, H_3L, ligand and its metal complexes.

No.	Complex	UV–Visible[a,b] (cm^{-1})	Magnetic moments (B.M.)		Conductance[a] $\Omega^{-1}\ cm^2\ mol^{-1}$
			μ_{compl}[d].	μ_{eff}[e].	
	H_3L	31746 (0.35), 28571 (0.2)	–	–	–
1	$[(L)Cr_2(OAc)_3(H_2O)_5]\cdot 3H_2O$	18484, 16611[c]	5.6	3.9	8.9
2	$[(H_2L)_2Mn(EtOH)_2]$	21277, 17301[c]	–	3.6	1.6
3	$[(L)Fe_2(NO_3)_3(H_2O)_5]\cdot 1.5H_2O$	16556[c]	8.3	5.9	4.8
4	$[(HL)_2Co_2]\cdot 0.5H_2O$	16611[c]	5.9	4.3	2.0
5	$[(HL)Ni_2(OAc)_2]\cdot 0.5EtOH$	20080, 16584[c]	5.1	3.78	1.7
6	$[(HL)Cu_2(OAc)_2]\cdot 0.5H_2O$	19685, 15337[c]	2.3	1.97	1.7
7	$[(H_2L)_2Zn]$	23585[c]	Diam.	Diam.	1.8
8	$[(H_2L)_2Cd(H_2O)_2]\cdot 3.5H_2O$	23753[c]	Diam.	Diam.	2.1
9	$[(H_2L)_2UO_2(H_2O)]$	23641, 21505 sh[c]	Diam.	Diam.	1.5

[a] Solutions in DMF (10^{-3} M).
[b] Values of ε_{max} are in parentheses and multiplied by 10^{-4} (L $mol^{-1}cm^{-1}$).
[c] Nujol mulls.
[d] $\mu_{compl.}$ is the total magnetic moments of all cations in the complex.
[e] $\mu_{eff.}$ is the magnetic moment of one cationic species in the complex.

3.2. Metal complexes

The synthesized metal complexes of Cr(III), Mn(II), Fe(III), Co(II), Ni(II), Cu(II), Zn(II), Cd(II) and UO_2(VI) ions with H_3L in the molar ratio 1:2 (L: M) possess characteristics colours with generally high decomposition temperatures (>300 °C) due to the coordination bonds (Table 1). They were found to be sparingly soluble in most organic solvents, but were soluble in DMF and non-hygroscopic. The obtained results of elemental analyses (C, H, N) are in good agreement with the calculated values of the proposed formulae. The magnetic moment values-recorded at room temperature for complexes-compete favorably with the calculated spin only magnetic values in most cases. The conductivity values of the metal complexes are very low, thus suggesting non-electrolytic character of the metal complexes.

3.2.1. IR spectra

The infrared spectral assignments of H_3L compared to its metal complexes are presented in Table 2. Comparison of the infrared spectrum of H_3L with the spectra of the metal complexes showed significant variation in the chromophoric absorption bands as a result of coordination. The broad band around 3432 cm^{-1}, which was assigned to ν(OH) stretching modes in H_3L was observed in the spectra of complexes coupled with increased broadness in the range 3255–3447 cm^{-1}. This observation was attributed to the effect of coordination of the oxygen atom of the OH group after deprotonation and/or coordinated or uncoordinated water molecules associated with the complexes. The strong band at 1567 cm^{-1}, attributed to $\nu(C=O) + \nu(C=C)$ vibrational stretching mode in H_3L, appeared in the spectra of the metal complexes at lower wave number. The intensities of the peaks were reduced as a result of coordination, which reduced the vibrational force of CO group upon coordination [27,28]. This interpretation is further emphasized by the negative slope of the linear relationship of ν C=O versus ν M-O as shown in Fig. 2, $\nu\ \bar{}^1_{M\text{-}O/cm} = 32361 - 20.65\ \nu\ \bar{}^1_{C=O/cm}$, $r = 0.99$, n = 6 points except Fe(III), Zn(II), Cd(II) and UO_2(VI) complexes, which means strong red shift of the stretching frequencies of $\nu_{C=O}$, with the shortness of M-O bond length (strong interaction). The azomethine group ν(C=N) band, which appeared as a medium peak at 1618 cm^{-1} in the spectrum of the ligand, appeared at slightly lower wave number for all complexes except for Mn(II), Zn(II), Cd(II) and UO_2(VI)-complexes. This indicates the involvement of the azomethine group in chelation in all complexes except those of Mn(II), Zn(II) and Cd(II) and UO_2(VI) ions [27,28]. This finding was supported by linear relationship of $\nu_{C=N}$ versus $\nu_{M\text{-}N}$, $\nu_{M\text{-}N} = 67188 - 41.512\ \nu_{C=N}$, $r = 0.95$, n = 5 points except **2**, **4**, **7**, **8** and **9**. The negative slope emphasized that the ligand coordinated with the metal ion *via* the azomethine group, ν(C=N). However, δ(C–N) deformation mode for all complexes was affected by coordination by shifting to much lower wave number when compared to that of the ligand due to the coordination, except for Mn(II), Zn(II), Cd(II) and UO_2(VI)-complexes, which display blue shift to higher wave number. The coordination modes of anions could be assigned from the extra vibrational bands; Cr(III)-complex **1** showed new bands at 1687 and 1576 cm^{-1}, which may be assigned to $\nu_{asym}(COO^-)$ and $\nu_{sym}(COO^-)$, respectively of the acetate group with band difference ($\Delta\nu = 111$ cm^{-1}), suggesting the monodentate nature of the acetate anion [29–31]. However, the acetato complexes **5** and **6** showed new bands in the ranges 1574–1586 and 1500–1507 cm^{-1} with differences (74 and 79 cm^{-1}) recognized to bidentate fashion of the

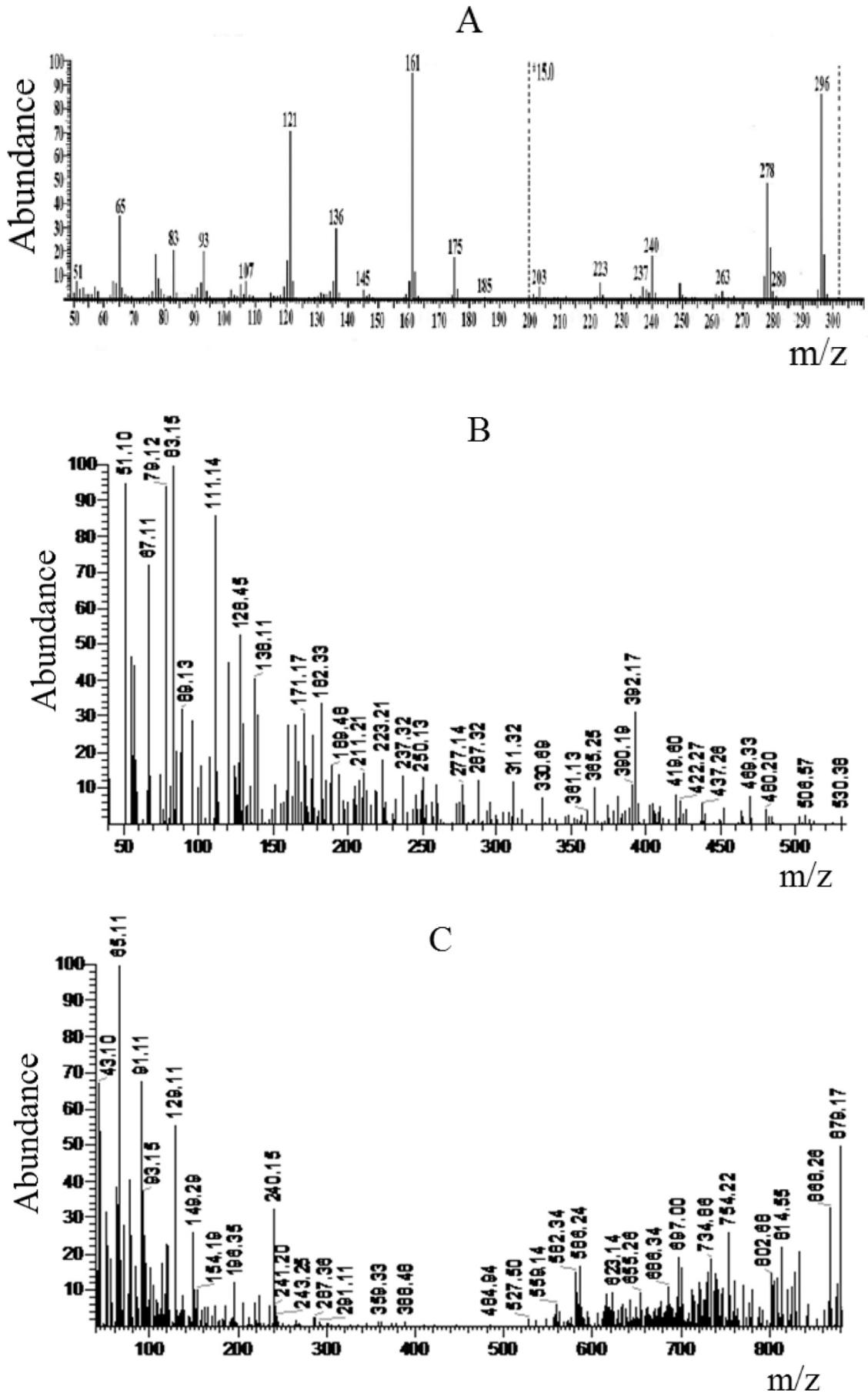

Fig. 1. Mass spectra of A: H_3L ligand, B: $[(HL)Ni_2(OAc)_2]\cdot 0.5EtOH$ (**5**) and C: $[(H_2L)_2UO_2(H_2O)]$ (**9**).

acetate group [32,33]. In complex **3**, the new bands observed at 1384 and 1152 cm^{-1}, may be assigned to the monodentate nature of the NO_3^- anion [34,35]. The dioxouranium(VI) complex **9** showed a strong band at 917 cm^{-1}, which may be assigned to the $\nu_3(UO_2)$ [29,36–38]. The value of ν_3 is used to calculate the force constant (F) of (O═U═O) by the method of McGlynn and Smith [39]. The calculated force constant for the complex is found to be 6.942 mdyn/Å. The U–O distance is also calculated by substitution in Jones relation [40]. The value of R_{U-O} is found to be 1.736 Å. The calculated F_{U-O} and R_{U-O} values are consistent with the reported range for the uranyl complexes [28,41]. The assignment of the proposed coordination sites is further supported by the appearance of new bands between 501 and 601 cm^{-1} and 419-494 cm^{-1}, which can be assigned to M - O and M - N bands, respectively [31,34,37,42].

3.2.2. Conductivity measurements

The molar conductivity values of the present metal complexes at room temperature (Table 3) are in the range 1.5–8.9 Ω^{-1} cm^2 mol^{-1} indicating for the non electrolytic nature of all complexes [43]. This finding is consistent with the infrared spectral data that showed the coordinated nature of acetate and nitrate anions.

3.2.3. Electronic spectra and magnetic moment measurements

Electronic spectra of the present metal complexes were examined for DMF solutions and/or Nujol mulls for sparingly soluble complexes. Comparison of the spectrum of the free ligand with its complexes showed the appearance of the bands of the ligand in all complexes with a slight blue or red shift in addition to new bands, which are listed in Table 3.

The electronic spectrum of the Cr(III) complex **1** showed two bands at 18,484 and 16,611 cm^{-1}, which may be assigned to $^4A_{2g}(F) \rightarrow {}^4T_{1g}(F)$ and $^4A_{2g}(F) \rightarrow {}^4T_{2g}(F)$ transitions, respectively in an octahedral geometry [44]. Whereas the third band, which is due to $^4A_{2g}(F) \rightarrow {}^4T_{1g}(P)$ transition, lies in the range of the ligand transitions that predicted at 35,666 cm^{-1}. The ligand field parameters of the current Cr(III) complex have been calculated using Tanab–Sugano diagrams B (579 cm^{-1}), 10Dq (1737 cm^{-1}) and β (0.56). The effective magnetic moment of the complex **1** is 3.9 B.M., which is consistent with the spin-only value for three unpaired electrons (3.87 B.M.) [45].

In case of Mn(II) complex **2** (d^5) high spin, spin allowed d-d transition is not expected due to the fact that such transitions are Laporte and spin forbidden. Thus, for Mn(II) complex, the intensities of transition from ground state to the state of four–fold multiplicity are very weak as compared with the ligand. However, the spectrum of the complex showed a weak band and a shoulder at 21,277 and 17,301 cm^{-1}, respectively. They were assigned to $^6A_{1g} \rightarrow {}^4T_{1g}(^4G)$ and $^6A_{1g} \rightarrow {}^4T_{2g}(^4G)$ transitions, respectively in an octahedral geometry [46,47]. The magnetic moment of the complex is 3.6 B.M. The lower value may be due to antiferromagnetic interaction [48]. The spectral data provide the ligand field parameters: B (960 cm^{-1}), 10Dq (3487 cm^{-1}) and β (0.97).

The electronic spectrum of the Fe(III) complex **3** showed one band at 16,556 cm^{-1}, within the range reported for octahedral complexes [49–51]. As a result of the strong charge transfer band, shadowing from UV-region to the visible region, it was difficult to recognize the type of the d–d transition [52]. The effective magnetic moment of the Fe(III) complex is 5.9 B.M., which is consistent with the presence of five unpaired electrons in the Fe(III) ion in an octahedral geometry [45].

The electronic spectrum of the Co(II) complex **4** showed one band at 16,611 cm^{-1}, which may be assigned to $^4A_2(F) \rightarrow {}^4T_1(P)$ transition in a tetrahedral geometry [53–55]. The effective magnetic moment of the complex is 4.3 B.M., which is close to the usual range for tetrahedral Co(II) complexes (4.4–4.8 B.M.) [45].

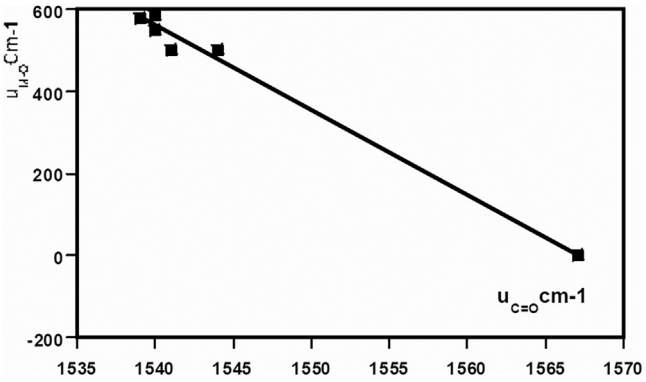

Fig. 2. Relation between ν(C═O) with ν(M - O) of metal complexes.

The electronic spectrum of the Ni(II) complex **5** showed two bands at 20,080 and 16,584 cm^{-1}, which may be assigned to the $^3T_1(F) \rightarrow {}^3T_1(P)$ transition in a tetrahedral geometry [44]. The effective magnetic moment of the Ni(II) complex is 3.78 B.M., which lies in the range (3.2–4.1 B.M.) reported for tetrahedral geometry [45].

The electronic spectrum of the Cu(II) complex **6** showed two bands at 19,685 and 15,337 cm^{-1}, which may be assigned to $^2B_{1g} \rightarrow {}^2E_g$ and $^2B_{1g} \rightarrow {}^2A_{1g}$ transitions in a square-planar geometry [56]. The effective magnetic moment of the Cu(II) complex is 1.97 B.M., which is consistent with one unpaired electron (d^9) [57]. X-band ESR spectrum of the Cu(II) complex, Fig. 3, was recorded in the solid state at 25 °C. The spectrum exhibits one broad band with g = 2.15 and the profile of the spectrum points to a square-planar geometry [58–61].

The electronic spectra of Zn(II) **7** and Cd(II) **8** complexes showed bands at 23,585 and 23,753 cm^{-1}, respectively, which may be attributed to charge transfer transitions. The complexes are diamagnetic as expected.

The electronic spectrum of the dioxouranium(VI) complex **9** showed two bands at 23,641 and 21,505 cm^{-1}. The higher energy band may be attributed to electronic transitions from apical oxygen atoms to *f* orbitals of the uranium(VI) ion and the lower energy band is due to charge transfer transition from equatorial ligand to the uranium(VI) ion [27]. The complex is diamagnetic as expected.

3.2.4. Thermal analysis

Thermal gravimetric analysis (TGA) is a precious technique to explore the nature of associated water or solvent molecules to be either in the inner or outer coordination sphere of the metal ion [62,63]. TGA and DTA data obtained for some of the current complexes (**3**–**6** and **9**), as representative examples, within the temperature range from ambient temperature up to 800 °C in an inert atmosphere, are listed in Table 4. The results of thermal analysis of these complexes (Table 4) are in good agreement with the theoretical formulae as suggested from elemental analyses.

In case of complex **3**, three decomposition stages were observed in the temperature range 32–265 (Scheme 2), which correspond to the loss of one and half non-coordinated water, two coordinated water and three coordinated water molecules in addition to a nitric acid molecule, respectively (weight loss; Calc./Found%; 3.81/3.69, 5.08/5.31 and 16.52/16.28%, respectively).

The thermogram of complex **5** showed two weight losses in the ranges 30–150 °C and 150–328 °C which correspond to half solvated ethanol and an acetic acid molecules (weight loss; Calc./Found%; 4.16/4.34 and 10.85/10.95%, respectively).

For complexes **4**, **6** and **9**, only one decomposition stage was interpreted. For complexes **4**, **6**, the decomposition stage was

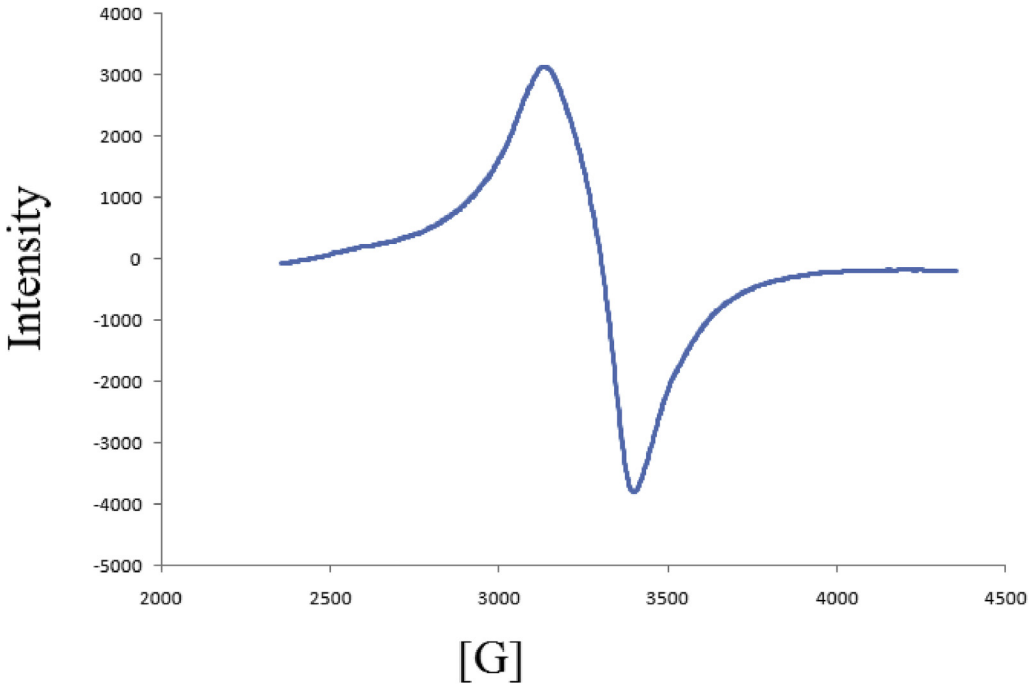

Fig. 3. X-band ESR spectrum of $[(HL)Cu_2(OAc)_2]\cdot 0.5H_2O$ (**6**).

Table 4
Thermal analyses data of some metal complexes of the Schiff base ligand.

Complex	Temperature range (°C)	% Wt. loss found/(calc.)	Lost fragment (No. of molecules)
$[(L)Fe_2(NO_3)_3(H_2O)_5]\cdot 1.5H_2O$ (**3**)	32–90	3.69/(3.81)	$1.5H_2O$ (hyd.)
	90–140	5.31/(5.08)	$2H_2O$ (coord.)
	140–265	16.28/(16.52)	$3H_2O$ (coord.) + 1 HNO_3
$[(HL)_2Co_2]\cdot 0.5H_2O$ (**4**)	30–125	1.28/(1.26)	$0.5H_2O$ (hyd.)
$[(HL)Ni_2(OAc)_2]\cdot 0.5EtOH$ (**5**)	30–150	4.34/(4.16)	0.5 EtOH (solv.)
	150–328	10.95/(10.85)	1 AcOH
$[(HL)Cu_2(OAc)_2]\cdot 0.5H_2O$ (**6**)	32–126	1.79/(1.64)	$0.5H_2O$ (hyd.)
$[(H_2L)_2UO_2(H_2O)]$ (**9**)	108–210	1.73/(2.05)	$1H_2O$ (coord.)

observed in the ranges 30–125 °C and 32–126 °C, corresponding to the loss of half non-coordinated water molecule (weight loss; Calc./Found%; 1.26/1.28 and 1.64/1.79% for complexes **4** and **6**, respectively). In complex **9**, the decomposition stage was observed in the range 108–210 °C, corresponding to the loss of one coordinated water molecule (weight loss; Calc./Found%; 2.05/1.73%). The activation parameters of the various decomposition stages were determined from the TG thermograms using the Costs-Redfern equations [64] in the following forms:

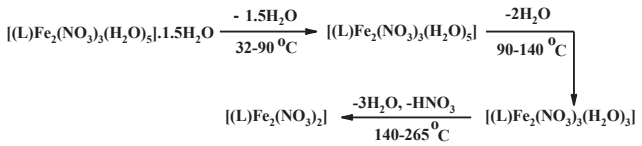

Scheme 2. Thermal degradation pattern of complex (**3**), $[(L)Fe_2(NO_3)_3(H_2O)_5]\cdot 1.5H_2O$.

$$\ln\left[1-(1-\alpha)^{1-n}\Big/(1-n)T^2\right] = M/T + B \quad \text{for } n \neq 1 \tag{1}$$

$$\ln\left[-\ln(1-\alpha)\Big/T^2\right] = M/T + B \quad \text{for } n = 1 \tag{2}$$

where M = -E/R and B = ln AR/Φ E; E, R, A and Φ are the heat of

Table 5
Temperatures of decomposition and kinetic parameters of some complexes.

Compound	Step	n order	T (K)	A (S^{-1})	Δ E (kJ mol^{-1})	ΔH (kJ mol^{-1})	ΔS (kJ mol^1K^{-1})	ΔG (kJ mol^{-1})
$[(L)Fe_2(NO_3)_3(H_2O)_5]\cdot 1.5H_2O$ **3**	First	1	344	34.1834	35.318	32.457	−0.224	77.159
	Second	0.5	393	50.760	48.530	45.263	−0.223	87.501
	Third	0.66	478	31.611	29.924	25.950	−0.228	109.214
$[(HL)_2Co_2]\cdot 0.5H_2O$ **4**	First	0.33	367	33.739	23.740	20.689	−0.226	82.850
$[(HL)Ni_2(OAc)_2]\cdot 0.5EtOH$ **5**	First	1	357	26.637	24.950	22.001	−0.227	80.559
	Second	0.66	539	16.891	19.688	15.205	−0.235	126.544
$[(HL)Cu_2(OAc)_2]\cdot 0.5H_2O$ **6**	First	1	336	30.504	28.816	26.023	−0.226	75.888
$[(H_2L)_2UO_2(H_2O)]$ **9**	First	1	460	19.717	18.030	14.210	−0.232	106.776

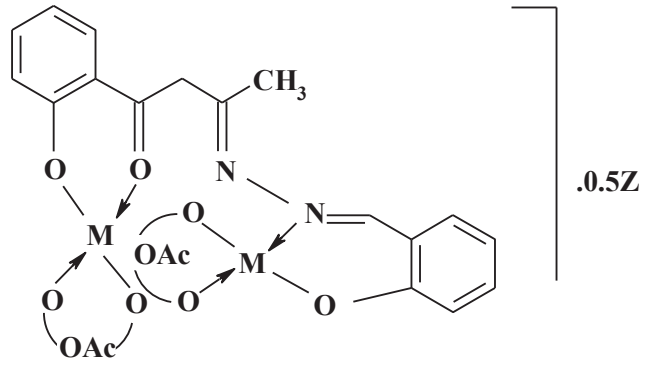

M	Z	Complex
Ni	EtOH	**5**
Cu	H_2O	**6**

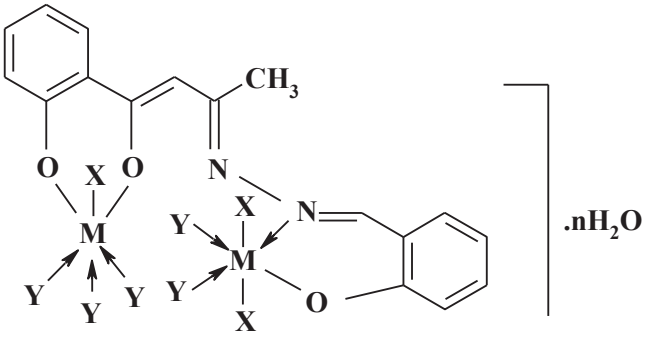

M	X	Y	n	Complex
Cr	OAc	H_2O	3	**1**
Fe	NO_3	H_2O	1.5	**3**

Scheme 3. Suggested structures of 1:2; L:M Cr(III), Fe(III), Ni(II) and Cu(II) complexes.

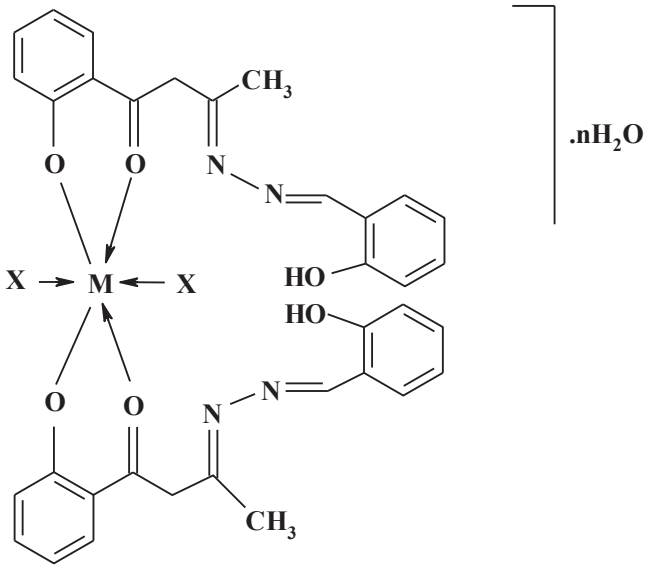

M	X	n	Complex
Mn	EtOH	nil	**2**
Zn	nil	nil	**7**
Cd	H_2O	3.5	**8**

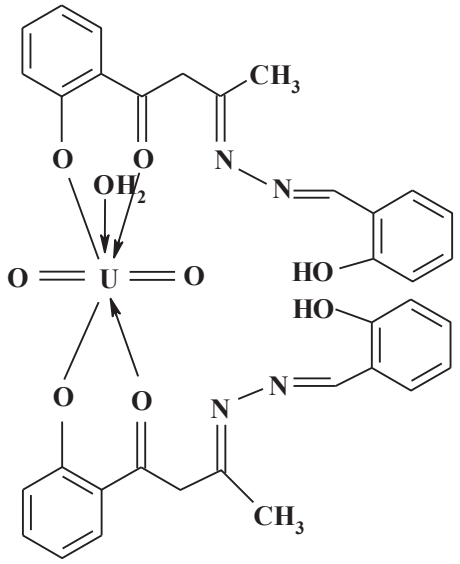

(9)

Scheme 4. Suggested structures of 2:1; L:M Mn(II), Zn(II), Cd(II) and UO_2(VI) complexes.

activation, the universal gas constant, pre-exponential factor and heating rate, respectively.

The correlation coefficient, *r*, was computed using the least square method for different values of $n = 0, 0.33, 0.5, 0.66, 1$ by plotting the left −hand side of Eq. (1) or (2) versus 1000/T. The *n* values which gave the best fit ($r \approx 1$). From the intercept and linear slope of such stage, the A and E values were determined. The other kinetic parameters ΔH, ΔS and ΔG were computed using the relationships; $\Delta H = E - RT$, $\Delta S = R[\ln(Ah/kT)\text{-}1]$ and $\Delta G = \Delta H - T\Delta S$, where k is the Boltzmann's constant and h is the Plank's constant. The kinetic parameters are listed in Table 5. The following remarks can be pointed out: (1) the positive values of ΔH* mean that the decomposition processes are endothermic. (2) The energy of activation values E_a for the second step of decomposition of complex **5** are lower than the first stage indicating that the rate of decomposition for this stage is higher than the first stage. In case of complex **3**, the second step of decomposition is higher than the first step. This confirms that the rate of decomposition for this stage is lower in the second step [65]. (3) The ΔS* values for complexes are found to be negative. This indicates that the activated complex is more ordered than the reactants and/or the reactions are slow [66]. (4) The values of ΔG* are relatively low and of positive sign indicating the autocatalytic effect of metal ions on thermal decomposition of the complexes and non−spontaneous processes [67].

3.2.5. Mass spectra

The mass spectra and the molecular ion peaks confirmed the proposed formulae of the complexes. Complexes **4**, **5**, **7** and **9** were chosen for mass spectral studies. Fig. 1 depicts the mass spectra of

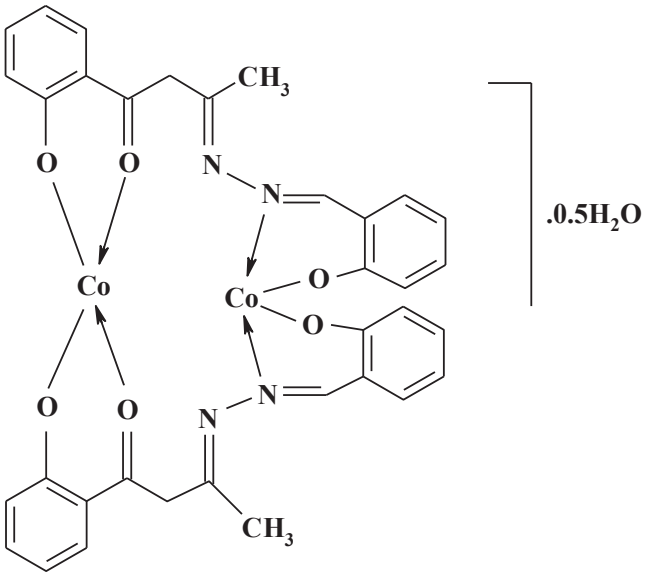

(4)

Scheme 5. Suggested structure of the 2:2; L:M Co(II) complex.

complexes **5** and **9**. Complexes **4** and **5** showed the molecular ion peaks at *m/z* 707 and 530, respectively which agree very well with the formula weights of the non-hydrated or non-solvated complexes; $[(HL)_2Co_2]$ (F. Wt = 706.5) and $[(HL)Ni_2(OAc)_2]$ (F. Wt = 529.86). This confirms the proposed structures of these complexes as 2:2 and 2:1; M:L complexes, respectively. Complexes **7** and **9** showed the molecular ion peaks at *m/z* 656 and 879, respectively which agree very well with the calculated formula weights of the complexes $[(H_2L)_2Zn]$ (F. Wt = 656.01) and $[(H_2L)_2UO_2(H_2O)]$ (F. Wt = 878.69), confirming their 1:2; M:L stoichiometry.

In the light of the preceding interpretation of different analytical and spectral data, the proposed structures of the metal complexes are represented in Schemes 3–5.

3.2.6. Molecular orbital calculations

The molecular structures were elucidated on the basis of the spectral, molar conductance, magnetic susceptibility and TGA data which indicated that the geometry of complexes were of octahedral, tetrahedral and square-planar conformations. Geometrically optimized structures of the free ligand and its metal complexes were obtained except uranyl-complex (**9**). Furthermore, the utility of quantum chemical descriptors such as heat of formation, dipole moment, hydration energy and frontier molecular orbitals (energy of the highest occupied molecular orbital and energy of the lowest unoccupied molecular orbitals) collected in Table 6 in elucidating the structure of complexes. Table 7 lists selected bond lengths of the optimized structures of the ligand and its metal complexes. It is well established that HOMO accounts for the electron donating ability while LUMO characterizes the ability to accept electron [36]. Also, high HOMO energy value infers that the molecule or ligand can easily release electrons to the unoccupied orbital of the metal ion, indicating strong binding affinity [36]. From the frontier molecular orbital approximation, high LUMO energy value infers that the molecule can easily accept electrons from the occupied orbital of the ligand, indicating strong binding affinity, $\nu_{C=O}/cm^{-1} = 1508.5–27.86\ E_{LUMO}/eV$, $r = 0.98$, n = 4 points, except complexes **1**, **2**, **4** and **8**. The negative slope emphasized that, increase the stability of the complex accompanied by the elongation of C=O (hypsochromic shift of the vibrational frequency). Furthermore, $E_{HOMO} = -6.351–0.0039\ \nu_{M\text{-}N}/cm^{-1}$, $r = 0.98$, n = 5, except complexes **1**, **3** and **7**, the negative slope indicates that increasing of E_{HOMO} relevance to weak stability of complex lead to red shift of the vibrational frequency of M - N bond.

However, the negative slope of the relationship of the calculated heat of formation (ΔH_f) versus $\nu_{C=N}$; $\Delta H_f/kcal.mol^{-1} = -59636 + 36.68\ \nu_{C=N}/cm^{-1}$, $r = 0.96$, n = 5, except complexes **3**, **6**, **7** and **9**, the positive slope refers to that more positive heat of formation (less stable) accompanied by less extent of red shift of the vibrational frequency of $\nu_{C=N}$.

Furthermore, the linear correlation between the calculated dipole moment (μ) versus the vibrational frequency of $\nu_{M\text{-}O}$, $\mu/D = -10.66 + 0.029\ \nu_{M\text{-}O}/cm^{-1}$, $r = 0.95$, n = 5 except complexes **2**, **4** and **7**, the positive slopes put forward increase of the μ values was accompanied by increasing the M - O bond strength.

3.3. Biological activity

3.3.1. Antimicrobial activity

The Schiff base ligand and its metal complexes were screened for antimicrobial activity against Gram positive bacteria (*S. aureus*; G+1 and *B. subtilis*; G+2), Gram negative bacteria (*S. typhimurium;* G-1 and *E. coli;* G-2) and fungi (*C. albicans;* F1 and *A. fumigates;* F2) and the results are listed in Table 8. The ligand is active against *A. fumigatus* only. It showed higher activity, which is comparable to that of cycloheximide. Against *S. aureus* and *E. coli*, all complexes are inactive except the Cr(III) complex, which showed a lower activity towards *S. aureus*. Against *B. subtilis*, some complexes are active and the order of activity is: Cu(II) > Ni(II) > Fe(III) > Cr(III) > Cd ≈ UO_2(VI). Against *S. typhimurium*, three complexes are active and the order of activity is: Ni(II) > UO_2(VI) > Cd(II). Against *C. albicans*, most of the complexes are active and the order of activity is: Ni(II) > UO_2(VI) > Fe(III) > Cr(III) > Cd(II) > Zn(II) > Cu(II) > Co(II).

Table 6
Structural parameters of the metal complexes.

No.	Complex	Total energy	Dipol moment	Heat of formation	Energy HOMO	Energy LUMO	E_{gap}	ED
	H_3L	−79886.47	1.726	−26.107	−8.959	−0.616	8.343	–
1	$[(L)Cr_2(OAc)_3(H_2O)_5]\cdot 3H_2O$	−180006.20	6.166	−766.350	−7.831	−1.322	6.509	100119.73
2	$[(H_2L)_2Mn(EtOH)_2]$	−196828.09	5.903	−206.971	−7.963	−0.699	7.264	116941.62
3	$[(L)Fe_2(NO_3)_3(H_2O)_5]\cdot 1.5H_2O$	−215213.04	6.555	−1064.90	−8.545	−1.269	7.276	135326.57
4	$[(HL)_2Co_2]\cdot 0.5H_2O$	−194938.05	8.960	−562.556	−8.266	−2.041	6.225	115051.58
5	$[(HL)Ni_2(OAc)_2]\cdot 0.5EtOH$	−167569.91	6.037	−622.290	−7.997	−1.179	6.818	87683.44
6	$[(HL)Cu_2(OAc)_2]\cdot 0.5H_2O$	−174102.06	4.164	−377.890	−8.022	−0.982	7.040	94215.59
7	$[(H_2L)_2Zn]$	−159645.19	3.258	31.197	−8.511	−0.734	7.777	79758.72
8	$[(H_2L)_2Cd(H_2O)_2]\cdot 3.5H_2O$	−174434.66	3.385	1.803475	−8.196	−0.899	7.297	94548.19
9	$[(H_2L)_2UO_2(H_2O)]$	38.3227	2.594	–	–	–	–	−79924.79

Table 7
Selected bond lengths of the optimized structures of transition metal complexes.

Atoms	Charges of atoms in complexes									
	H_3L[1]	Cr	Mn	Fe	Co	Ni	Cu	Zn	Cd	UO_2
C-Oa_1	1.354	1.360	1.360	1.360	1.339	1.343	1.313	1.299	1.286	1.356
C=Oa_1	1.226	1.363	1.364	1.361	1.283	1.276	1.269	1.261	1.252	1.499
C-Oa_2	–	–	1.360	–	1.331	–	–	1.299	1.310	1.355
C=Oa_2	–	–	1.234	–	1.344	–	–	1.260	1.220	1.505
C-$O_{(OAc)bi}$	–	–	–	–	–	1.344	1.321	–	–	–
C-$O_{(OAc)bi}$	–	–	–	–	–	1.276	1.256	–	–	–
C=N_1	1.299	1.513	–	1.541	1.365	1.317	1.317	–	–	–
C=N_2	–	–	–	–	1.316	–	–	–	–	–
C-Ob_1	1.368	1.357	–	1.363	1.370	1.361	1.355	–	–	–
C-Ob_2	–	–	–	–	1.354	–	–	–	–	–
M-Oa_1	–	1.910	1.852	1.899	1.905	1.840	1.859	1.953	2.211	2.145
M=Oa_1	–	1.906	1.858	1.895	2.029	1.856	1.894	2.035	2.204	2.155
M-Oa_2	–	–	1.871	–	1.911	–	–	1.954	2.211	2.141
M=Oa_2	–	–	2.214	–	1.907	–	–	2.034	2.209	2.148
M-$O_{(NO3)}$	–	–	–	1.905	–	–	–	–	–	–
M-$O_{(OAc)mo}$	–	1.904	–	–	–	–	–	–	–	–
M-$O_{(OAc)bi}$	–	–	–	–	–	1.869	1.921	–	–	–
M-$O_{(OAc)bi}$	–	–	–	–	–	1.850	1.901	–	–	–
M-N_1	–	1.924	–	1.906	1.869	1.856	1.973	–	–	–
M-N_2	–	–	–	–	1.883	–	–	–	–	–
M-Ob_1	–	1.898	–	1.916	1.841	1.842	1.899	–	–	–
M-Ob_2	–	–	–	–	1.840	–	–	–	–	–
M-$O_{H2O,EtOH}$	–	1.905	2.252	1.907	–	–	–	–	2.206	2.152
M-O_{UO2}	–	–	–	–	–	–	–	–	–	2.155

1-(C-Oa_1, C=Oa_1): O atoms of *o*-acetoacetylphenol in all complexes.
2-(C-Oa_2, C=Oa_2): O atoms of *o*-acetoacetylphenol in 1:2 and 2:2; M:L complexes.
3-(C-Ob_1, C-Ob_2): O atoms of salicylaldehyde hydrazone in case of 2:1 and 2:2; M:L complexes.
4-(N_1, N_2): bonded N atoms to metal in 2:1 and 2:2; M:L complexes.
5-(M-Oa_1, M=Oa_1): O atoms of *o*-acetoacetylphenol in all complexes.
6-(M-Oa_2, M=Oa_2): O atoms of *o*-acetoacetylphenol in 1:2 and 2:2; M:L complexes.
7-(M-Ob_1, M-Ob_2): O atoms of salicylaldehyde hydrazone in case of 2:1 and 2:2; M:L complexes.

Finally, four complexes are active against *A. fumigatus* and the order of activity is: Fe(III) > UO_2(VI) > Ni(II) > Zn(II) with promising activity of the Fe(III) complex.

It was interest in elucidating the microbial activity to find a correlation of Frontier orbitals energy HOMO, LUMO and E_{gab}, with the biological activity of the screened organisms yielding: E_{HOMO}/eV = −7.715−0.0495 G +2, r = 0.975, n = 4, except complexes **3** and **9**. The negative slope refers to decreasing the biological activity toward Gram positive with the increasing of E_{HOMO}, which is related to weak stability of complexes.

Table 8
Antimicrobial activity of the Schiff base ligand and its metal complexes.

Organism	Mean[a] of zone diameter, nearest whole mm.											
	Gram - positive bacteria				Gram - negative bacteria				Yeasts and Fungi[b]			
	Staphylococcus aureus (ATCC 25923)		*Bacillus subtilis* (ATCC 6635)		*Salmonella typhimurium* (ATCC 14028)		*Escherichia coli* (ATCC 25922)		*Candida albicans* (ATCC 10231)		*Aspergillus fumigatus*	
Sample	Concentration											
	1 mg/ml	0.5 mg/ml	1 mg/ml	0.5 mg/ml	1 mg/ml	0.5 mg/ml	1 mg/ml	0.5 mg/ml	1 mg/ml	0.5 mg/ml	1 mg/ml	0.5 mg/ml
H_3L	–	–	–	–	–	–	–	–	–	–	31 H	27 H
$[(L)Cr_2(OAc)_3(H_2O)_5]\cdot 3H_2O$ (**1**)	7 L	8 L	9 L	8 L	–	–	–	–	19 I	16 I	–	–
$[(H_2L)_2Mn(EtOH)_2]$ (**2**)	–	–	–	–	–	–	–	–	–	–	–	–
$[(L)Fe_2(NO_3)_3(H_2O)_5]\cdot 1.5H_2O$ (**3**)	–	–	16 I	14 I	–	–	–	–	21 I	17 I	34 H	29 H
$[(HL)_2Co_2]\cdot 0.5H_2O$ (**4**)	–	–	–	–	–	–	–	–	9 L	7 L	–	–
$[(HL)Ni_2(OAc)_2]\cdot 0.5EtOH$ (**5**)	–	–	17 I	14 I	16 I	13 I	–	–	27 H	23 H	23 H	20 H
$[(HL)Cu_2(OAc)_2]\cdot 0.5H_2O$ (**6**)	–	–	28 H	25 H	–	–	–	–	11 L	9 L	–	–
$[(H_2L)_2Zn]$ (**7**)	–	–	–	–	–	–	–	–	12 I	9 L	10 L	7 L
$[(H_2L)_2Cd(H_2O)_2]\cdot 3.5H_2O$ (**8**)	–	–	9 L	7 L	9 L	7 L	–	–	15 I	12 I	–	–
$[(H_2L)_2UO_2(H_2O)]$ (**9**)	–	–	9 L	7 L	11 L	8 L	–	–	21 I	18 I	25 H	20 H
Control[c]	35	26	35	25	36	28	38	27	35	28	37	26

– = No effect.
L: Low activity = Mean of zone diameter ≤1/3 of mean zone diameter of control.
I: Intermediate activity = Mean of zone diameter ≤2/3 of mean zone diameter of control.
H: High activity = Mean of zone diameter >2/3 of mean zone diameter of control.
[a] Calculated from 3 values.
[b] Identified on the basis of routine cultural, morphological and microscopical characteristics.
[c] Chloramphenicol in the case of Gram-positive bacteria, cephalothin in the case of Gram-negative bacteria and cycloheximide in the case of fungi.

Table 9
Antitumor activity of the Schiff base ligand and its nickel(II) and copper(II) complexes against HepG2 cell line.

Compound	IC $_{50}$ (μg/ml)
H_3L	113
$[(HL)Ni_2(OAc)_2]\cdot 0.5EtOH$ (**5**)	89.1
$[(HL)Cu_2(OAc)_2]\cdot 0.5H_2O$ (**6**)	120
Doxorubicin	0.47

IC $_{50}$ = inhibition concentration 50%.

However, E_{gap}, which is related to stability of complexes, is linearly correlated with the biological activity toward the current microorganism: $E_{gap}/eV = 6.248 + 0.1114\ F_1$, $r = 0.99$, n = 5, except complexes **3**, **4**, **7** and **9** and $E_{gap}/eV = 6.248 + 0.11136$ G+2, $r = 0.98$, n = 4, except complexes **3** and **9.** The positive slope reveals that the biological activity is enhanced towards Gram positive and fungi with increasing the stability of the complex.

3.3.2. *Antitumor activity*

The anticancer activity of the Schiff base ligand and its Ni(II) and Cu(II) complexes was determined *in vitro* against human cancer cell line liver Carcinoma (HEPG2). Table 9 schedules the values of IC_{50}, compared with the standard drug doxorubicin. The ligand and its complexes showed lower activity and the order of activity is as follows: Ni(II) complex > H_3L ligand > Cu(II) complex. The difference in activity of the complexes indicates that the type of ion may be the reason for the different anticancer activity [68].

4. Conclusion

A new Schiff base ligand was synthesized and characterized. Reactions of the ligand with chromium(III), manganese(II), iron(III), cobalt(II), nickel(II), copper(II), zinc(II), cadmium(II) and dioxouranium(VI) ions yielded mono and binuclear complexes that were characterized by elemental and thermal analyses, spectroscopic methods (IR, electronic, ESR and mass spectra), molar conductivity and magnetic moment measurements. Mononuclear complexes (with 1:2; M:L molar ratio) were obtained in case of manganese(II), zinc(II), cadmium(II) and dioxouranium(VI) ions while binuclear complexes (with 2:1; M:L molar ratio) were obtained in case of chromium(III), iron(III), nickel(II) and copper(II) ions and with 2:2; L:M in case of cobalt(II) ion. The outer compartment of the ligand is used in coordination in mononuclear complexes. In addition to the outer compartment, the azomethine nitrogen and phenolic oxygen are involved in coordination in binuclear complexes. Different geometrical structures were proposed for metal complexes such as octahedral structure for Cr(III), Mn(II), Fe(III) and Cd(II) complexes, tetrahedral for Co(II) and Ni(II) complexes, square-planar for Cu(II) complex while in Zn(II) and dioxouranium(VI) complexes, the metal ions are tetra- and hepta-coordinate, respectively. Kinetic parameters of the thermal decomposition stages have been evaluated using Coats–Redfern equations. The molecular parameters of the ligand and its metal complexes have been calculated and correlated with the experimental data. The antimicrobial activity of the ligand and its complexes was investigated. The antitumor activity of the ligand and its Ni(II) and Cu(II) complexes was investigated against HepG2 cell line.

Appendix A. Supplementary data

Supplementary data related to this article can be found at http://dx.doi.org/10.1016/j.molstruc.2017.01.012.

References

[1] D.N. Dhar, C.L. Taploo, J. Sci. Ind. Res. 41 (1982) 501–506.
[2] A. Jarrahpour, D. Khalili, E. De Clercq, C. Salmi, J.M. Brunel, Molecules 12 (2007) 1720–1730.
[3] M. Salehi, F. Rahimifar, M. Kubicki, A. Asadi, Inorg. Chim. Acta 443 (2016) 28–35.
[4] N. Raman, S. Sobha, L. Mitu, Monatsh Chem. 143 (2012) 1019–1030.
[5] H. Chang, L. Jia, J. Xu, T. Zhu, Z. Xu, R. Chen, T. Ma, Y. Wang, W. Wu, J. Mol. Struct. 1106 (2016) 366–372.
[6] S.A. Al-Harbi, M.S. Bashandy, H.M. Al-Saidi, A.A.A. Emara, T.A.A. Mousa, Spectrochim. Acta A 145 (2015) 425–439.
[7] H. Wu, G. Pan, Y. Bai, H. Wang, J. Kong, F. Shi, Y. Zhang, X. Wang, J. Coord. Chem. 66 (2013) 2634–2646.
[8] Y. Harinath, D.H.K. Reddy, B.N. Kumar, Ch Apparao, K. Seshaiah, Spectrochim. Acta A 101 (2013) 264–272.
[9] M.S. Alam, J.H. Choi, D.U. Lee, Bioorg. Med. Chem. 20 (2012) 4103–4108.
[10] K.S. Kumar, S. Ganguly, R. Veerasamy, E. De Clercq, Eur. J. Med. Chem. 45 (2010) 5474–5479.
[11] S.B. Desai, P.B. Desai, K.R. Desai, Heterocycl. Commun. 7 (2001) 83–90.
[12] (a) D. Chen, A.E. Martell, Inorg. Chem. 26 (1987) 1026–1030;
(b) J. Costamagna, J. Vargas, R. Latorre, A. Alvarado, G. Mena, Coord. Chem. Rev. 119 (1992) 67–88.
[13] S.A. Gaballa, S.M. Asker, S.A. Barakat, S.M. Teleb, Spectochim. Acta A 67 (2007) 114–121.
[14] H. Keypour, M. Shayesteh, M. Rezaeivala, F. Chalabian, L. Valencia, Spectrochim. Acta A 101 (2013) 59–66.
[15] P.A. Vigato, S. Tamburini, Coord. Chem. Rev. 248 (2004), 1717–2128.
[16] S.A. Duclos, H. Stoeckli-Evans, T.R. Ward, Helv. Chim. Acta 84 (2001) 3148–3161.
[17] H. Golchoubian, A. Nemati Kharat, Pol. J. Chem. 79 (2005) 825–830.
[18] (a) A. Ghaffarinia, H. Golchoubian, R. Hosseinzadeh, J. Chin. Chem. Soc. 52 (2005) 531–534;
(b) H. Okawa, H. Furutachi, D.E. Fenton, Coord. Chem. Rev. 144 (1998) 51–75;
(c) D.E. Fenton, U. Casellato, P.A. Vigato, M. Vidali, Inorg. Chim. Acta 95 (1984) 187–193.
[19] S.M.E. Khalil, K.A. Bashir, J. Coord. Chem. 55 (2002) 681–696.
[20] S.M. El-Medani, M.M. Aboaly, H.H. Abdalla, R.M. Ramadan, Spectrosc. Lett. 37 (2004) 619–632.
[21] H.A. Flaschka, EDTA Titration, second ed., Pergamon Press, 1964.
[22] A.I. Vogel, Textbook of Quantitative Inorganic Analysis, fourth ed., Longman, London, 1978.
[23] T.S. West, Complexometry with EDTA and Related Reagents, third ed., DBH Ltd., Pools, 1969.
[24] F.E. Mabbs, D.I. Machin, Magnetism and Transition Metal Complexes, Chapman and Hall, London, 1973.
[25] (a) A.W. Bauer, W.W.M. Kirby, J.C. Sherris, M. Turck, Am. J. Clin. Pathol. 45 (1966) 493–496;
(b) D.C. Gross, S.E. De Vay, Physiol. Plant Pathol. 11 (1977) 13–28.
[26] (a) T. Mosmann, J. Immunol. Methods 65 (1983) 55–63;
(b) A.P. Wilson, in: J.R.W. Masters (Ed.), Cytotoxicity and Viability Assay in Animal Cell Culture: a Practical Approach, third ed., Oxford University Press, 2000.
[27] M. Shebl, S.M.E. Khalil, S.A. Ahmed, H.A.A. Medien, J. Mol. Struct. 980 (2010) 39–50.
[28] M. Shebl, Spectrochim. Acta A 117 (2014) 127–137.
[29] S.M.E. Khalil, M. Shebl, F.S. Al-Gohani, Acta Chim. Slov. 57 (2010) 716–725.
[30] G.M. Abu El-Reash, O.A. El-Gammal, A.H. Radwan, Spectrochim. Acta A 121 (2014) 259–267.
[31] M. Shebl, M.A. El-ghamry, S.M.E. Khalil, M.A.A. Kishk, Spectrochim. Acta A 126 (2014) 232–241.
[32] M. Shebl, Spectrochim. Acta A 70 (2008) 850–859.
[33] B.A. El-Sayed, M.M. Abo Aly, A.A.A. Emara, S.M.E. Khalil, Vibr. Spec. 30 (2002) 93–100.
[34] M. Shebl, S.M.E. Khalil, Monatsh. Chem. 146 (2015) 15–33.
[35] M. Shebl, M.A. Ibrahim, S.M.E. Khalil, S.L. Stefan, H. Habib, Spectrochim. Acta A 115 (2013) 399–408.
[36] O.M.I. Adly, A. Taha, S.A. Fahmy, J. Mol. Struct. 1054–1055 (2013) 239–250.
[37] M. Shebl, J. Coord. Chem. 69 (2016) 199–214.
[38] S.M.E. Khalil, J. Coord. Chem. 49 (1999) 45–61.
[39] S.P. McGlynn, J.K. Smith, W.C. Neely, J. Chem. Phys. 35 (1961) 105–116.
[40] L.H. Jones, Spectrochim. Acta A 10 (1958) 395–403.
[41] M. Shebl, J. Mol. Struct. 1128 (2017) 79–93.
[42] G.G. Mohamed, E.M. Zayed, A.M.M. Hindy, Spectrochim. Acta A 145 (2015) 76–84.
[43] W.J. Geary, Coord. Chem. Rev. 7 (1971) 81–122.
[44] J.C. Bailar, H.J. Emeleus, R. Nyholm, A.F. Trotman-Dickenson, Comprehensive Inorganic Chemistry, vol. 3, Pergamon Press, 1975.
[45] F.A. Cotton, G. Wilkinson, Advanced Inorganic Chemistry. A Comprehensive Text, fourth ed., John Wiley and Sons, New York, 1986.
[46] S.M.E. Khalil, J. Coord. Chem. 56 (2003) 1013–1024.
[47] R.M. Issa, S.A. Azim, A.M. Khedr, D.F. Draz, J. Coord. Chem. 62 (2009) 1859–1870.
[48] K.A.R. Salib, S.L. Stefan, S.M. Abu El-Wafa, H.F. El-Shafiy, Synth. React. Inorg.

Met. Org. Chem. 31 (2001) 895–915.
[49] M. Shebl, J. Coord. Chem. 62 (2009) 3217–3231.
[50] M. Shebl, M. Saif, A.I. Nabeel, R. Shokry, J. Mol. Struct. 1118 (2016) 335–343.
[51] A.A.A. Emara, B.A. El-Sayed, E.A.E. Ahmed, Spectrochim. Acta A 69 (2008) 757–769.
[52] M. Shebl, S.M.E. Khalil, F.S. Al-Gohani, J. Mol. Struct. 980 (2010) 78–87.
[53] O.A. El-Gammal, A.A. El-Asmy, J. Coord. Chem. 61 (2008) 2296–2306.
[54] H.S. Seleem, B.A. El-Shetary, M. Shebl, Heteroat. Chem. 18 (2007) 100–107.
[55] A.A.A. Emara, O.M.I. Adly, Trans. Met. Chem. 32 (2007) 889–901.
[56] M.M. Abd-Elzaher, S.A. Moustafa, A.A. Labib, M.M. Ali, Monatsh. Chem. 141 (2010) 387–393.
[57] M. Shebl, S.M.E. Khalil, A. Taha, M.A.N. Mahdi, Spectrochim. Acta A 113 (2013) 356–366.
[58] M. Shebl, Spectrochim. Acta A 73 (2009) 313–323.
[59] S.M.E. Khalil, H.S. Seleem, B.A. El-Shetary, M. Shebl, J. Coord. Chem. 55 (2002) 883–899.
[60] O.M.I. Adly, Spectrochim. Acta A 79 (2011) 1295–1303.
[61] O.M.I. Adly, A.A.A. Emara, Spectrochim. Acta A 132 (2014) 91–101.
[62] M. Shebl, H.S. Seleem, B.A. El-Shetary, Spectrochim. Acta A 75 (2010) 428–436.
[63] M. Shebl, S.M.E. Khalil, A. Taha, M.A.N. Mahdi, J. Mol. Struct. 1027 (2012) 140–149.
[64] A.W. Coats, J.P. Redfern, Nature 201 (1964) 68–69.
[65] A.H.M. Siddaligaiah, S.G. Naik, J. Mol. Struct. 582 (2002) 129–136.
[66] C.R. Vinodkumar, M.K.M. Nair, P.K. Radhakrishnan, J. Therm. Anal. Cal. 61 (2000) 143–149.
[67] U. El- Ayaan, I.M. Gabr, Spectrochim. Acta A 67 (2007), 263–2723.
[68] N. El-wakiel, M. El-keiy, M. Gaber, Spectrochim. Acta A 147 (2015) 117–123.